Research Square

Preprints are preliminary reports that have not undergone peer review.
They should not be considered conclusive, used to inform clinical practice,
or referenced by the media as validated information.

Deep eutectic solvent-impregnated cellulose triacetate matrix as a dual- function platform for selective preconcentration and colorimetric detection of Ni(II) ions

Nisha Yadav
University of Delhi
Kalyan Yakkala
ykalyan@es.du.ac.in
University of Delhi
Ashok K. Pandey
Kishinchand Chellaram College, HSNC University

Article

Keywords: Deep eutectic solvent, Membrane optode, Colorimetric detection, Nickel(II) preconcentration, Cellulose triacetate matrix, Environmental water monitoring

Posted Date: October 27th, 2026

DOI: https://doi.org/10.21203/rs.3.rs-11280337/v1

License: This work is licensed under a Creative Commons Attribution 4.0 International License.
Read Full License

Additional Declarations: No competing interests reported.

Deep eutectic solvent-impregnated cellulose triacetate matrix as a dual-function platform for selective preconcentration and colorimetric detection of Ni(II) ions

Nisha Yadav[1], Kalyan Yakkala[1*], and Ashok K. Pandey[2]

[1]Department of Environmental Studies, University of Delhi, Delhi-110007, India

[2]Department of Nuclear and Radiochemistry, Kishinchand Chellaram College, HSNC University, Mumbai-400020, India

Abstract

Monitoring of Ni(II) in environmental waters is essential given its toxicity and widespread occurrence, yet conventional analytical techniques are equipment-intensive, time-consuming and poorly suited to routine monitoring. This study reports a colorimetric membrane optode for Ni(II). The optode was fabricated by immobilizing a deep eutectic solvent (DES), prepared from tetrabutylammonium chloride and decanoic acid (1:1 mole ratio), together with 1-(2-pyridylazo)-2-naphthol (PAN) in a cellulose triacetate (CTA) matrix. The DES acted as both extractant and plasticizer, so no separate additives were needed. At the optimized pH of 6, the membrane changed from yellow to magenta within 30 min, with maximum absorbance at 568 nm. The optode exhibited a linear response over 0.05–2.5 μg/mL Ni(II), with a detection limit of 0.03 μg/mL, and showed good selectivity over competing ions. FTIR, DSC, TGA, FESEM-EDX and AFM confirmed hydrogen bonding within the DES, the thermal stability of the membrane and the uptake of Ni(II) in the optode matrix. Results for river water, industrial wastewater, electroplating wastewater and open-drain water agreed with ICP-MS, with deviations of 1.25–9.72% for spiked samples. The DES–CTA optode therefore offers a simple, selective platform for the simultaneous preconcentration and optical detection of Ni(II) in water samples.

Keywords: Deep eutectic solvent, Membrane optode, Colorimetric detection, Nickel(II) preconcentration, Cellulose triacetate matrix, Environmental water monitoring.

* Corresponding author.

E-mail address: ykalyan@es.du.ac.in ; kalyan.yk@gmail.com (Kalyan Yakkala)

Introduction

Rapid population growth and industrial expansion have accelerated the release of toxic heavy metals into aquatic environments, posing significant risks to ecosystem integrity and human health. Among several pollutants, nickel enters the environment through both natural weathering and a wide range of anthropogenic activities and predominantly persists in its +2 oxidation state[1]. Even trace levels of nickel in surface water and groundwater can produce marked toxicological effects, and the World Health Organization (WHO) has set the maximum permissible limit for nickel in drinking water at 0.07 mg L^{-1}[2]. Chronic human exposure to nickel through water and food is associated with allergic reactions, cardiovascular and renal disease, pulmonary fibrosis, and nasal and lung cancers, with the nervous system representing a principal target of nickel toxicity[3]. Continuous, reliable monitoring of nickel in water bodies is therefore essential for environmental protection and public-health surveillance. Conventional instrumental techniques can determine nickel at trace levels, but they are laboratory-based and time-consuming, and require sophisticated, costly instrumentation and skilled personnel[4–7].

Ni(II) ions are usually present at trace concentrations within complex aqueous matrices, and a preconcentration step is generally indispensable for achieving adequate sensitivity and selectivity[8]. Established microextraction-based preconcentration strategies, including dispersive liquid–liquid microextraction (DLLME), liquid-phase microextraction (LPME), cloud-point extraction (CPE), hollow-fiber liquid-phase microextraction (HF-LPME), and dispersive solid-phase extraction (DSPE), are efficient but typically involve multiple manipulation steps and organic solvent extraction. In addition, a separate analytical procedure is required for final quantification in purified aqueous samples[9–13]. This has driven growing interest in compact, fast and self-contained colorimetric sensors with one-step sample preparation that can serve as first-line monitoring tools or early-warning alarms for water quality monitoring[14]. Membrane optodes offer this possibility.

Membrane optodes, prepared by immobilizing a chromogenic reagent within a plasticized polymer matrix, are well suited to simple, on-site monitoring. The interaction of the target analyte with the embedded reagent produces a distinctive, quantifiable optical response that combines high selectivity and sensitivity with a broad calibration range[15–17]. A further practical advantage of optode-based sensing is the simultaneous preconcentration of the analyte at the membrane surface with minimal sample handling[18]. Functionally, an optode comprises two elements: a receptor that recognizes the target analyte and a transducer that converts this recognition event into a measurable optical signal[19]. Ionic liquids have frequently been

employed as carriers within such membranes to mediate analyte extraction[20], but their broader adoption is constrained by intrinsic toxicity, poor biocompatibility, and high cost[21], creating demand for greener alternative solvents/carriers capable of selectively isolating toxic metal ions from complex matrices, such as industrial wastewater.

Deep eutectic solvents (DES), formed through hydrogen-bonding interactions between a hydrogen-bond acceptor (HBA) and a hydrogen-bond donor (HBD), have emerged as greener substitutes for ionic liquids owing to their simple preparation, tuneable physicochemical properties, and comparatively benign environmental impact[22]. Their favourable solvation behaviour, structural tunability, and inherently low toxicity have made DES increasingly prominent in metal ion extraction and separation[23]. Their use is not limited to conventional liquid–liquid extraction. Aqueous two-phase systems (ATPS) prepared from choline chloride/urea and betaine/urea DES together with dipotassium hydrogen phosphate have recently been shown to selectively partition hexavalent chromium into the DES-rich phase while lead, cobalt, nickel and cadmium are retained in the salt-rich phase, providing a low-cost, non-flammable alternative to polymer- or ionic-liquid-based ATPS[24]. In a related study, natural deep eutectic solvents prepared from betaine and fructose were combined with ultrasound-assisted liquid–liquid microextraction to preconcentrate Ni(II) and Cu(II) simultaneously from tea and water samples prior to FAAS determination, with recoveries above 96% and sub-µg/L detection limits[25]. DES-mediated extraction is understood to proceed through several possible interaction mechanisms, including hydrogen bonding, van der Waals forces, electrostatic interactions, hydrophobicity, π–π interactions, redox reactions, and Lewis acid–base interactions, depending on the analyte and the DES components involved[23]. Owing to this tunability and their low environmental impact, DES are increasingly used as membrane components in place of conventional ionic liquids[26].

Several DES formulations have accordingly been explored for nickel separation from environmental and industrial matrices. Sakamoto et al. prepared a hydrophobic DES from decanoic acid and trialkyl methylammonium chloride to leach and recover battery metals from nickel laterite ore. The hydrophobic character of this DES enabled selective stripping and scrubbing of Ni, Mn and Co while excluding Fe, and avoided the liquid–liquid extraction step conventionally required with volatile organic solvents[27]. Rashid et al. developed natural deep eutectic solvents from a quaternary ammonium salt and an organic acid to extract nickel ions from contaminated mangrove soil[28]. Carreira et al. proposed a hydrophobic DES composed of decanoic acid and trioctylphosphine oxide as an HCl super-concentrator for the one-pot

leaching of spent lithium-ion battery cathodes with simultaneous Ni(II) precipitation[29]. Tan et al. used a DES-based simultaneous complexation and preconcentration (DES-SCP) method, in which the DES extractant was combined with dithizone as a chelating ligand, to preconcentrate nickel from Antarctic lake-water samples prior to FAAS determination[30]. Elahi et al. reported a hydrophobic DES liquid–liquid microextraction procedure based on tetrabutylammonium chloride and decanoic acid (1:2) for the simultaneous preconcentration of Ni(II) and Zn(II) prior to FAAS analysis[31]. Zinov'eva et al. proposed a hydrophobic DES based on di(2-ethylhexyl) phosphoric acid and menthol for the extraction of Al(III), Ni(II) and Cu(II) from aqueous solution[32]. Erbas et al. combined a tetrabutylammonium chloride–decanoic acid DES with sodium diethyldithiocarbamate complexation for the microextraction and preconcentration of nickel prior to micro-sampling FAAS determination in water and food samples[33]. Sorouraddin et al. developed a dispersive liquid–liquid microextraction method using a hydrophobic DES formed from choline chloride and 4-aminophenol for the determination of Co(II) and Ni(II) in river water, well water, urban water, and fruit-juice samples[34], and Rad et al. used a choline chloride/4-bromophenol DES in a dispersive liquid–liquid microextraction procedure for nickel preconcentration and separation from water samples[35]. Optode membranes can also combine sensing with removal. A phenanthraquinone monophenyl thiosemicarbazone-doped cellulose triacetate optode was recently used both to detect mercury(II) colorimetrically and to adsorb it quantitatively from cucumber, fish, soil and water samples, and could be regenerated with nitric acid and reused over several months[36]. This dual capability motivated the use of a DES-based extractant, rather than a conventional plasticizer alone, in the membrane developed in the present study.

Indicator dyes play a central role in the preparation of membrane optodes, as they generate the optical response arising from interaction with the analyte. Organic chromogenic reagents such as 1,5-diphenylcarbazide (DPC), 4-(2-pyridylazo)resorcinol (PAR), 4-(2-thiazolylazo)-resorcinol (TAR), 1-(2-pyridylazo)-2-naphthol (PAN), dithizone, 2-(5-bromo-2-pyridylazo)-5-diethylaminophenol (Br-PADAP), and thiosemicarbazone derivatives[15,16,36–40], have been incorporated into optode membranes through various immobilization strategies, in combination with a suitable extractant/carrier, where they mediate extraction of the target metal ion into the sensing layer and generate an optical signal proportional to its concentration. Coupling an extractant (carrier), such as a DES, with such indicator dyes has been shown to enhance the selectivity and sensitivity of the resulting optode relative to solution spectrophotometry using the same dye alone[15,40].

The objective of the present work is to develop a deep eutectic solvent-based membrane optode by immobilizing 1-(2-pyridylazo)-2-naphthol (PAN) within a cellulose triacetate polymer matrix for the determination of Ni(II). The DES used to construct the optode was prepared from tetrabutylammonium chloride (TBACl) as the hydrogen-bond acceptor and decanoic acid (DecA) as the hydrogen-bond donor in a 1:1 molar ratio. The DES and the DES-loaded membrane optode were characterized by FTIR, FESEM-EDX, DSC, TGA and AFM analyses, and the membrane was optimized with respect to pH, working range, and response time. Upon adsorption of Ni(II), the optode undergoes a visible colour change from yellow to magenta, with λ_{max} = 568 nm and a response time of 30 min at pH 6. The adsorption of Ni(II) was further characterized using isotherm and kinetic models. The selectivity of the optode for Ni(II) over competing metal ions was evaluated in multi-ion solutions, and the optode was applied to the determination of Ni(II) in real environmental water samples.

Materials and methods

Chemicals and reagents

All the reagents used were of analytical grade. Cellulose triacetate (CTA), tetrabutylammonium chloride (TBACl) and decanoic acid (DecA) were obtained from Sigma-Aldrich (USA). Dichloromethane (DCM) and 1-(2-pyridylazo)-2-naphthol (PAN) were obtained from Merck (Mumbai, India). Distilled water purified with an ELGA LC197 system was used throughout. Nickel(II) chloride was used to prepare the stock and standard solutions. pH adjustments were carried out using dilute hydrochloric acid (HCl) and sodium hydroxide (NaOH).

Instrumentation

A miniature Flame UV-visible spectrophotometer (Ocean Insight, USA) was used to measure the absorbance of the optode sample (2 cm × 1 cm) placed inside a quartz cell (3 cm × 1 cm). A Hanna HI2210 pH meter (Hanna Instruments, USA) was used for pH measurements. Infrared spectra were recorded on a Nicolet iS50 FTIR spectrometer (Thermo Fisher Scientific, USA) within the range of 400-4000 cm^{-1}. The FESEM study was carried out with Zeiss Gemini SEM 500 thermal field emission Scanning Electron microscope (Carl Zeiss, Germany). For the morphology study, Atomic Force Microscopy was performed in non-contact mode by Park system NX 10 AFM (Park systems, South Korea). Thermogravimetric analysis (TGA) of the membrane was carried out using TA TGA 5500 (TA Instruments, USA). The melting point of the prepared DES was measured by Q200 modulated DSC (TA instruments, USA) with mass flow control, and the DES mixtures were stirred using a Tarsons SPINOT^{TM} digital magnetic

stirrer hotplate (Tarsons, India). The adsorption studies were carried out using FHM 32 ARCOS III Inductively Coupled Plasma Optical Emission Spectrometry (ICP-OES) instrument (SPECTRO Analytical Instruments GmbH, Germany). The concentration of Ni(II) in real water samples was determined using a triple quadrupole Inductively Coupled Plasma Mass Spectrometry (ICP-MS) instrument Agilent 8900 ICP-QQQ (Agilent Technologies, USA). Energy Dispersive X-Ray Fluorescence (EDXRF) measurements were carried out using ARL™ QUANT'X EDXRF Spectrometer (Thermo Scientific™, USA). An ultrasonicator (Labman, UK) was used to homogenize the casting solutions.

Preparation of Hydrophobic Deep Eutectic Solvent

Hydrophobic DES were prepared by mixing TBACl (hydrogen-bond acceptor) and DecA (hydrogen-bond donor) in three molar ratios (1:1, 1:2 and 2:1). The weighed components were placed in glass vials, stirred and heated on a Tarsons SPINOT™ digital magnetic stirrer hotplate at 80˚C for 60 min[41]. The resulting viscous liquids were cooled to room temperature and kept for 24 h before use in optode preparation.

Preparation of Membrane Optode

The optode was prepared following the protocol described previously by our group[15]. The base polymer, CTA (0.2 g), was dissolved in 7 mL of DCM. Solutions of PAN (0.001 g) and the prepared DES (0.2 g) were prepared separately in glass vials. After the solutions were combined, the mixture was ultrasonicated to obtain a homogeneous mixture. The obtained casting mixture was poured into a 9-cm diameter Petri dish with a lid and placed on a level surface for 2 days to allow controlled evaporation of solvent. After the membrane was formed, it was peeled off and washed thoroughly with distilled water to remove any soluble components. Membrane optode pieces of 2 cm × 1 cm were used throughout.

Spectrophotometry

The formation of the Ni–PAN complex in the membrane optode and the intensity of the resulting colour change were studied spectrophotometrically. The membrane optode (2 cm × 1 cm) was equilibrated for 30 min in different pH solutions ranging from pH 1 to pH 10 containing a known concentration of Ni(II) and the absorbance was recorded at λ_{max}=568 nm. All the pH adjustments were performed using dilute solutions of HCl and NaOH.

In order to understand the kinetics, the optode sample was equilibrated for a pre-determined time in solutions containing 1 µg/mL and 2.5 µg/mL Ni(II), and the absorbance was recorded

spectrophotometrically at λ_{max}=568 nm. The steps from optode preparation to absorbance measurement are illustrated in Fig.1.

Adsorption isotherm studies

The adsorption of Ni(II) onto the membrane optode was studied through ICP-OES by quantifying the concentration of Ni(II). For this, the membrane optode was equilibrated in 25 mL of aqueous Ni(II) solutions of known concentration. The amount of Ni(II) adsorbed, q (mg/g) was calculated using the equation:

$$q = \frac{C_o - C_e}{m} \times V \quad (1)$$

Where, C_o (µg/mL) and C_e (µg/mL) are the concentration before and after adsorption of Ni(II) respectively, m (g) is the weight of the membrane optode used and V(L) is the final volume of the solution containing Ni(II).

An adsorption isotherm describes the equilibrium relationship between the solute adsorbed on the surface of the membrane optode and its concentration present in the aqueous solution and is widely used to evaluate the type of adsorption and the capacity of the adsorbent. The data obtained in the present work were fitted to the Langmuir and Freundlich isotherm models to understand the adsorption behaviour of the prepared membrane optode.

Langmuir Isotherm

The Langmuir isotherm is an equilibrium adsorption isotherm model which assumes monolayer adsorption on a homogeneous surface[42]. The linearized Langmuir equation is expressed as:

$$\frac{C_e}{q} = \frac{1}{ab} + \frac{C_e}{b} \quad (2)$$

Freundlich Isotherm

The Freundlich isotherm is an empirical model that assumes multilayer adsorption on a heterogeneous surface and is useful for describing physical adsorption[42]. The Freundlich isotherm is expressed as:

$$\log q = \log K + \frac{1}{n} \log C_e \quad (3)$$

In both models, q(mg/g) corresponds to the amount of Ni(II) adsorbed on the surface of the membrane optode, n is the Freundlich constant, K(mg/g) $(L/mg)^{1/n}$ is the Freundlich empirical

constant, C_o is the concentration of Ni(II) before adsorption, C_e is the concentration of Ni(II) in the aqueous solution after the adsorption onto the surface of the membrane optode, m (g) is the weight of the membrane optode, V(L) is the final volume of the aqueous solution used, *a* (L/mg) is the adsorption constant for Langmuir, and *b* (mg/g) is the maximum (monolayer) adsorption capacity.

Adsorption kinetics

Adsorption kinetics describes the rate of adsorption and the mechanism by which the adsorbate is transferred from the aqueous solution to the adsorbent surface over time until equilibrium is reached. The rate of adsorption depends on the interaction between the adsorption sites on the adsorbent surface and the adsorbate[43]. In the present work, both pseudo-first-order and pseudo-second-order kinetic models were applied to understand the adsorption process.

Pseudo-first order kinetics

The pseudo-first-order model assumes that the rate of adsorption is proportional to the number of unoccupied sites, so that the uptake rate decreases as the sites are filled[44]. The pseudo-first-order equation is expressed as:

$$\log(q_e - q_t) = \log q_e - k_1 t \quad (4)$$

Pseudo-second order kinetics

The pseudo-second-order model assumes that the rate is controlled by chemical interaction between the adsorbate and the adsorbent surface[45]. The pseudo-second-order equation is expressed as:

$$\frac{t}{q_t} = \frac{1}{k_2 {q_e}^2} + \frac{t}{q_e} \quad (5)$$

Where, k_1(min^{-1}) is the pseudo-first-order rate constant, k_2 (g mg^{-1} min^{-1}) is the pseudo-second-order rate constant, and q_e (mg g^{-1}) and q_t (mg g^{-1}) are the adsorption capacity at equilibrium and at time t (min), respectively.

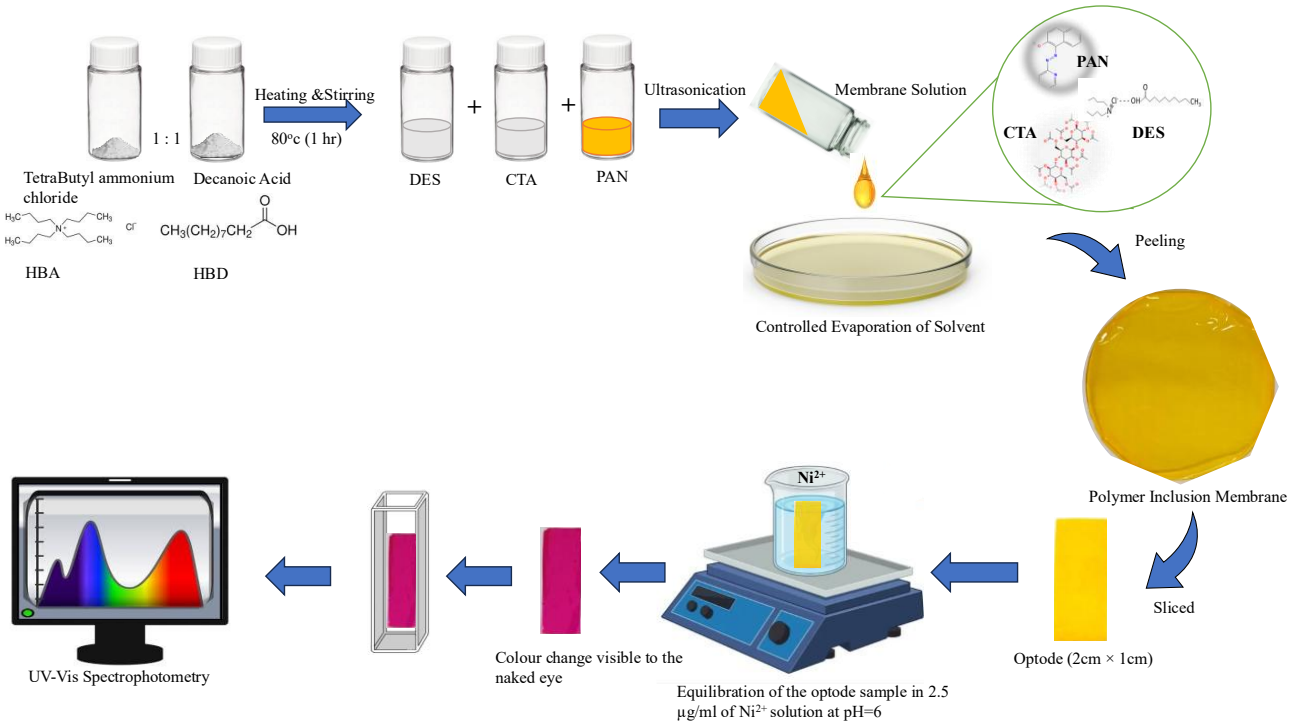


Fig. 1. Steps from optode preparation to absorbance measurement.

Results and discussion

Formation of optode

Different amounts of the polymer matrix, CTA (0.1–0.3 g), were investigated to obtain a mechanically stable and flexible membrane. The amount of the chromophore PAN, immobilized in the CTA matrix for its ability to chelate transition metals such as Ni(II), was also varied. At a lower amount of PAN, reduced complexation was observed, and at a higher amount, the absorbance exceeded 2, which lies outside the reliable range of most spectrophotometers. An optimal amount was therefore selected that gave the maximum absorbance within the measurable range.

Hydrophobic deep eutectic solvents (HDES) consisting of TBACl and DecA were prepared in three molar ratios (1:1, 1:2 and 2:1). All three were transparent; the 2:1 DES was highly viscous, whereas the other two had the desired consistency (Table S1). Five optodes (M1–M5) were prepared with different amounts of the same components, and their responses towards Ni(II) are compiled in Table S2.

All the prepared membranes exhibited good mechanical strength and flexibility, indicating that the HDES can function as both an extractant and a plasticizer, thereby eliminating the need for an additional plasticizer. Optode M2, which contained twice the amount of PAN, showed an absorbance greater than 2 at 568 nm. Therefore, it was not selected. Optode M3 showed a good response towards Ni(II) uptake, as shown in Fig. S1, but the response was much slower than that of M1. Optode M4 showed a slow and unsatisfactory response. Optode M5, prepared without DES, did not respond to Ni(II), indicating that the DES facilitates the transfer of Ni(II) into the membrane and the formation of the Ni–PAN complex. Optode M1 changed colour rapidly from yellow to magenta in the presence of Ni(II) and gave the maximum absorbance. Therefore, optode M1, consisting of 0.2 g CTA, 0.2 g DES (1:1) and 0.001 g PAN, was chosen for further study. The chemical structures of the optode components are given in Fig. S2.

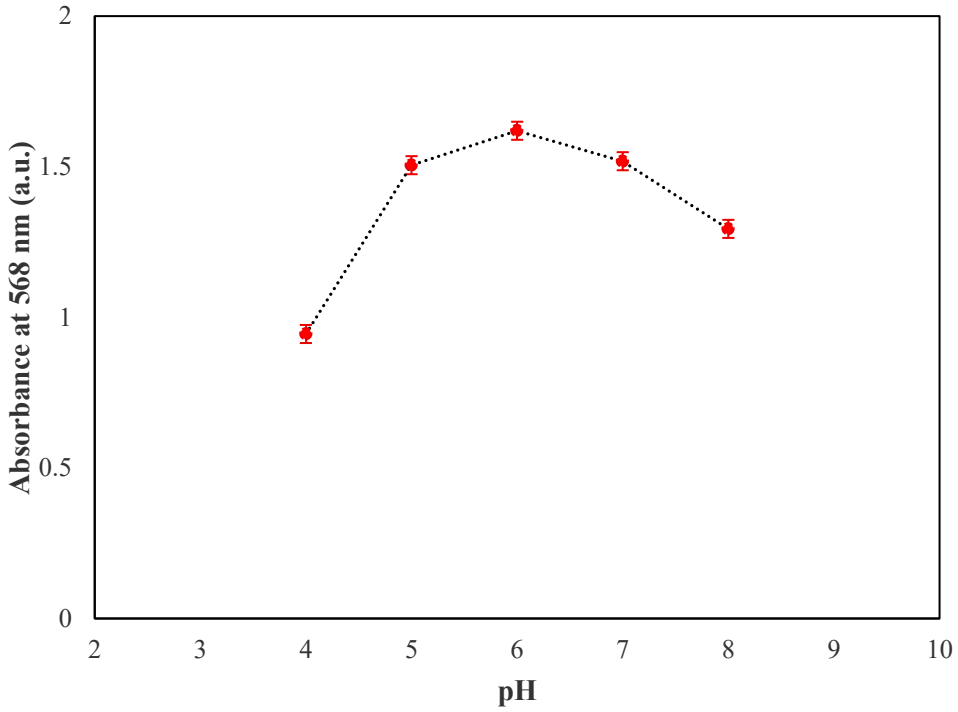
Effect of pH and contact time

The pH is an important parameter that affects the overall complexation and response of the membrane towards Ni(II). The response of the membrane optode was studied across a wide pH range. The membrane optodes of uniform size (2 cm × 1 cm) were used. At pH 1, there was complete leaching of PAN in the solution. At pH 2, the colour changed from yellow to light orange. The prominent colour change started from pH 3 onwards, where the optode changed from yellow to magenta. However, at pH 3, the response was very slow, and it took 1 hr to show the visible colour change. The rapid colour response appeared from pH 4 onwards. As seen from Fig. 2(a), the maximum absorbance of the Ni–PAN complex was observed at pH 6. Above pH 6, the absorbance decreased up to pH 8, which may be attributed to the hydrolysis of Ni(II)[46]. Therefore, pH 6 was selected for all subsequent experiments.

Response time

The response-time study was carried out to determine the effect of contact time between the DES-loaded membrane optode and Ni(II) in solution. The membrane optode was equilibrated in well-stirred Ni(II) solutions (1 and 2.5 µg/mL) at pH 6, and its absorbance was recorded at different time intervals. The response increased with time until the absorbance reached a constant value, indicating maximum uptake. The equilibration time was 30 min and did not vary between the two Ni(II) concentrations (Fig. 2(b)). The absorbance remained almost constant after 30 min, indicating that equilibrium had been reached. Thus, a 30 min response time was chosen for further studies.

(a)



(b)

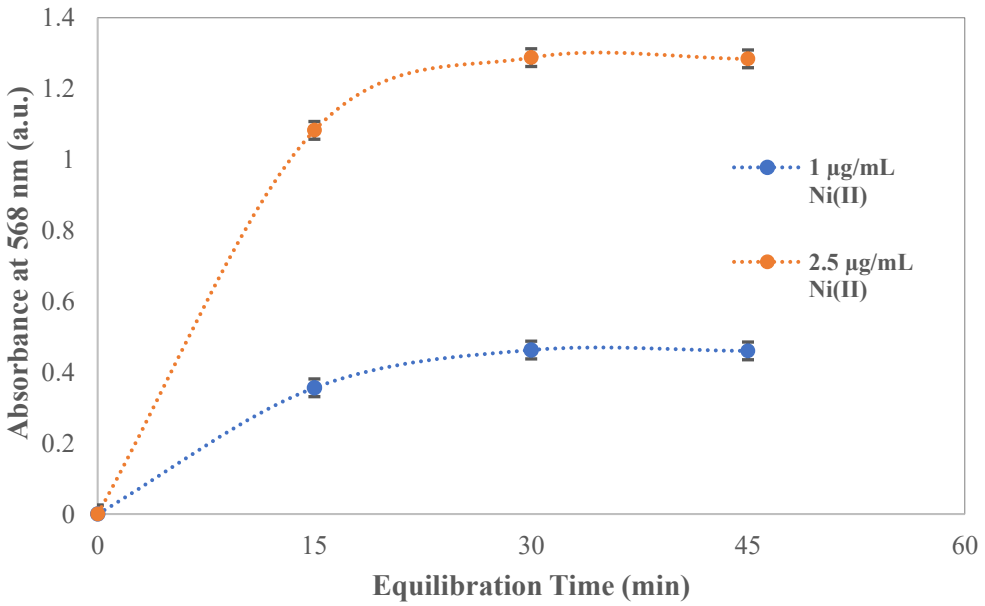


Fig. 2. (a) Effect of pH on the absorbance of the optode equilibrated with 2.5 µg/mL Ni(II), (b) absorbance of the membrane at 568 nm as a function of equilibration time with 1 and 2.5 µg/mL Ni(II) at pH 6.

Linearity, working range and optical response of the optode

The response of the developed membrane optode towards Ni(II) was studied at pH 6 with a contact time of 30 min in Ni(II) solutions ranging from 0.05 µg/mL to 2.5 µg/mL. After

equilibration, the absorbance of each membrane was measured. The blank membrane showed maximum absorbance at 470 nm, corresponding to PAN in the DES–CTA matrix[47]. With increasing Ni–PAN complexation at higher Ni(II) concentrations, the peak shifts to 568 nm and the absorbance reaches about 1.3 at 2.5 µg/mL.

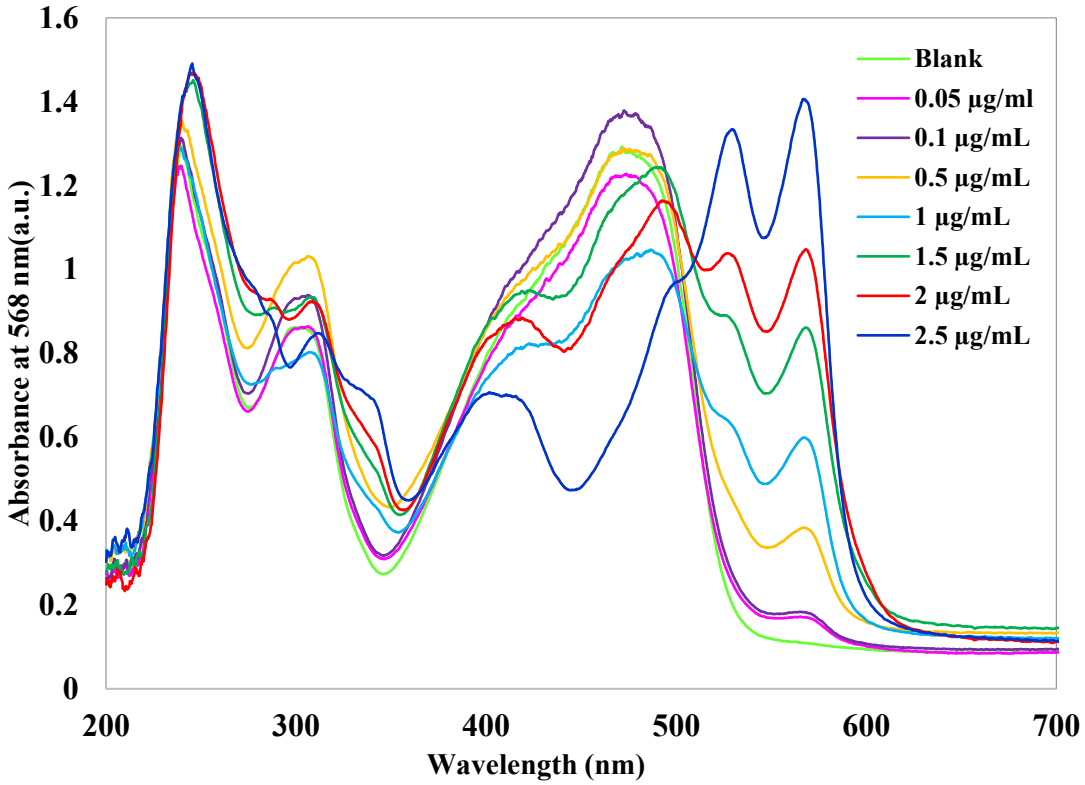
The spectra of the blank and Ni(II)-loaded membranes (Fig. 3(a)) show the shift from 470 nm to 568 nm on PAN–Ni(II) complexation; similar observations were reported by Wei et al[48].

The UV-visible spectra of membranes equilibrated with Ni(II) at concentrations from 0.05 µg/mL to 2.5 µg/mL were recorded from 200 to 700 nm (Fig. 3(a)). The absorbance increased systematically from 0.05 µg/mL to 2.5 µg/mL, indicating a direct relationship between Ni(II) concentration and absorbance.

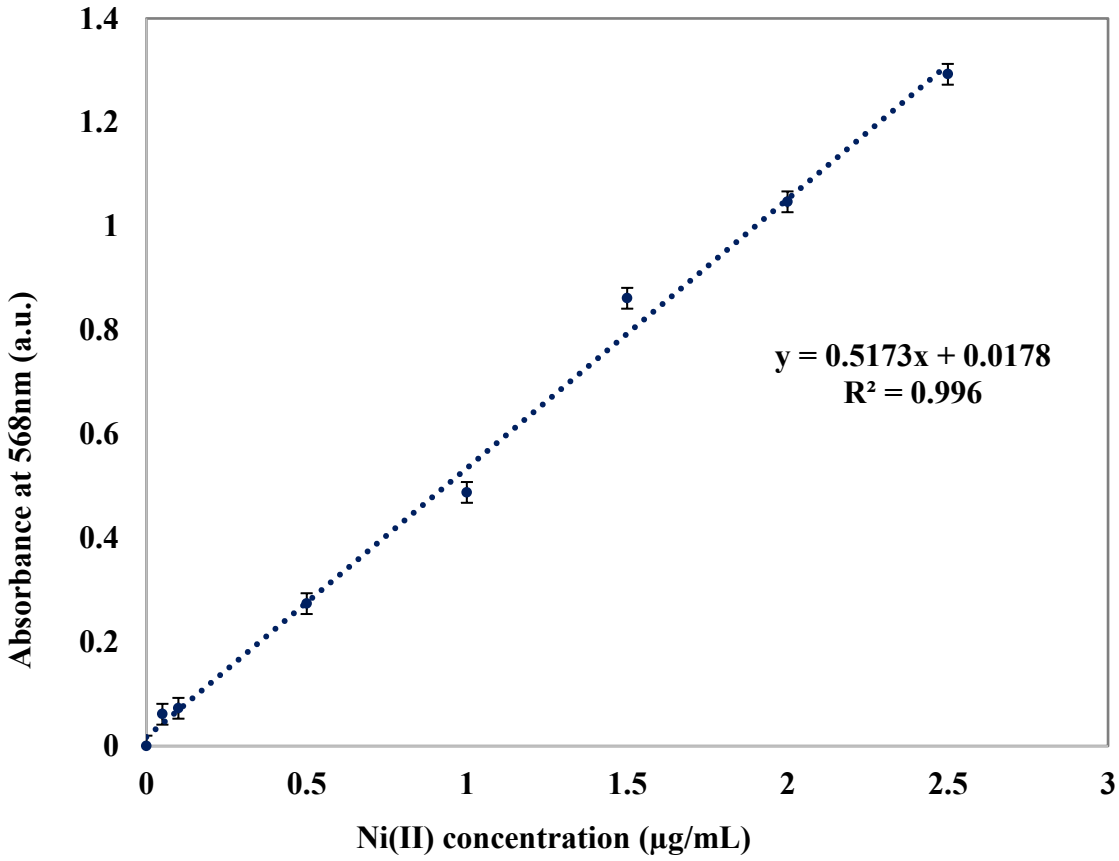
A calibration curve was constructed to evaluate the relationship between absorbance and Ni(II) concentration (Fig. 3(b)). The slope of the regression line (0.517 mL/µg) represents the sensitivity of the method, and the small intercept (0.018) can be attributed to the background absorbance of the membrane. The correlation coefficient ($R^2 = 0.996$) indicates good linearity, so the calibration can be used for the determination of Ni(II) in environmental and industrial samples. The response of the membrane was linear from 0.05 µg/mL to 2.5 µg/mL Ni(II) at pH 6, with a limit of detection (LOD) of 0.03 µg/mL.

With increasing Ni(II) concentration, the membrane colour changed progressively from yellow to magenta (Fig. 3(c)).

(a)


Absorbance at 568 nm(a.u.)
Wavelength (nm)
Blank
0.05 µg/ml
0.1 µg/mL
0.5 µg/mL
1 µg/mL
1.5 µg/mL
2 µg/mL
2.5 µg/mL

(b)


Absorbance at 568nm (a.u.)
Ni(II) concentration (µg/mL)
y = 0.5173x + 0.0178
R² = 0.996

(c)

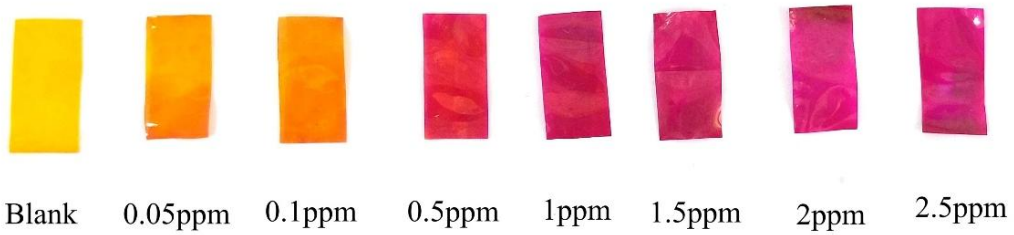


Fig. 3. (a) UV-visible spectra of membrane optodes equilibrated with different concentrations of Ni(II) ions at pH 6, (b) calibration curve for Ni(II) obtained spectrophotometrically after 30 min equilibration at pH 6, (c) Change in colour of the membrane samples as a function of Ni(II) concentrations in the equilibrating aqueous solutions.

Quantification of Ni(II) ions using EDXRF

Membrane optodes of equal weight (0.012 g) were equilibrated with Ni(II) solutions from 0.05 µg/mL to 2.5 µg/mL to determine the minimum Ni(II) concentration that produces a discernible EDXRF peak. The EDXRF spectra exhibited characteristic nickel emission at approximately 7.47 keV and 8.26 keV, assigned to the Ni K_α and K_β emission lines[49]. As shown in Fig. S3(a,b), the nickel signal increased with Ni(II) concentration in the sample matrix.

Physical and chemical characterization

FTIR Spectroscopy

FTIR spectroscopy was used to examine the functional groups and hydrogen bonding in the prepared DES and the membrane optode before and after Ni(II) uptake. The FTIR spectra of DecA, TBACl and the TBACl:DecA (1:1) DES are given in Fig. 4(a), and the characteristic absorption bands with their peak assignments are compiled in Table S3. The C-H stretching bands at 2957 cm^{-1} and 2869 cm^{-1} in TBACl and at 2917 cm^{-1} and 2851 cm^{-1} in DecA appear as an overlapped envelope at 2917 cm^{-1} and 2861 cm^{-1} in the spectrum of the 1:1 DES, with no major change, as expected since the alkyl chains are not directly involved in the interaction. Similar results were reported by Zhuocheng et al.[50]

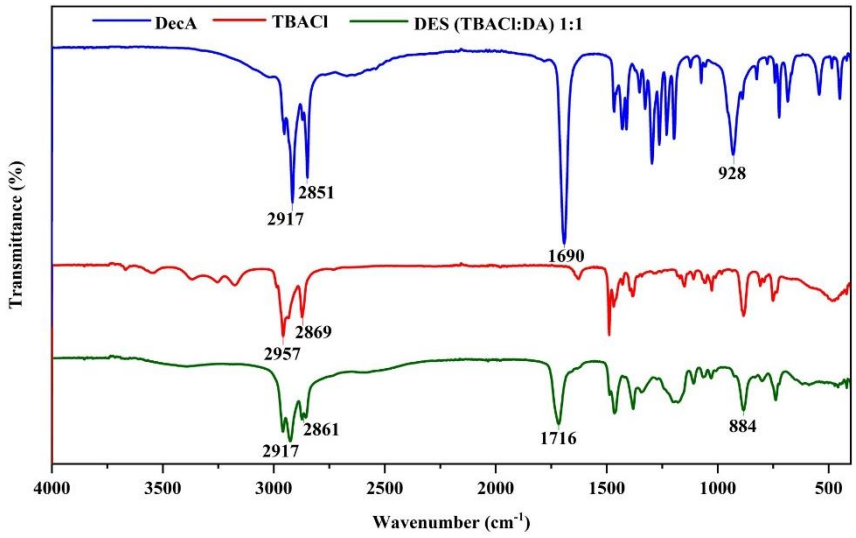
The broad O-H stretching band of DecA (≈2500–3300 cm^{-1}) is weakened and broadened in the DES spectrum owing to hydrogen bonding between the carboxylic O-H group and the chloride anion of TBACl, which replaces the cyclic DecA dimers. The C=O stretching band of DecA at 1690 cm^{-1} shifts to 1716 cm^{-1} upon DES formation ($\Delta\nu$ = +26 cm^{-1}), consistent with disruption of the hydrogen-bonded DecA dimers and the formation of O-H···Cl^- hydrogen bonds with TBACl.[51] Furthermore, in the DecA spectra, the out-of-plane O-H bending band of the dimer at 928 cm^{-1} is no longer observed in the DES spectrum, indicating loss of the dimer structure.[50,52] The band at 884 cm^{-1} in the DES coincides with a band of TBACl (≈880 cm^{-1}) arising from skeletal/C-N^+ vibrations of TBA^+, and is therefore not assigned to DecA. A weak, broad feature near 3400 cm^{-1} in the DES is attributed to residual moisture, since TBACl is hygroscopic. Thus, the FTIR spectra support the hydrogen-bond formation between TBACl and DecA in the DES.

The FTIR spectra of the membrane optode with and without Ni(II) are given in Fig. 4(b), and the absorption bands with their peak assignments and $\Delta\nu$ values are listed in Table S4. In Fig. 4(b), the C-H stretching vibrations, which indicate the presence of organic hydrocarbons, show only a +1 cm^{-1} change (2926 to 2927 cm^{-1}), which is within the spectral resolution. The peak at 1739 cm^{-1} in the blank membrane, which represents the ester C=O stretching, did not show any shift after loading with Ni(II). The C-O stretching peaks at 1216 cm^{-1} and 1034 cm^{-1} in the blank membrane change by only −4 and −2 cm^{-1} (to 1212 and 1032 cm^{-1}) in the loaded membrane, again within the spectral resolution. Together with the C=O band at 1739 cm^{-1}, these bands are characteristic of the acetate ester groups of the membrane matrix. A low-wavenumber peak at 601 cm^{-1} that remains unchanged both before and after loading can be

attributed to the O-C=O deformation of the acetate group of the matrix, it is not specific to PAN.

The band positions change by only 0–4 cm^{-1} (Table S4). These differences are within the spectral resolution of the measurement (state resolution, e.g., 4 cm^{-1}) and are therefore not considered significant shifts. The lower overall intensity of the loaded-membrane spectrum is attributed to differences in film thickness and contact with the ATR crystal rather than to a chemical change. Because the Ni(II)-PAN complex is present only in trace amounts at the Ni(II) concentration used (2.5 µg/mL), its characteristic bands (pyridyl C=N, azo N=N, phenolic C-O and M-N/M-O vibrations) are not expected to be resolved against the dominant matrix bands. The FTIR results therefore show that the acetate-ester membrane matrix remains chemically unchanged after Ni(II) uptake.

(a)



(b)

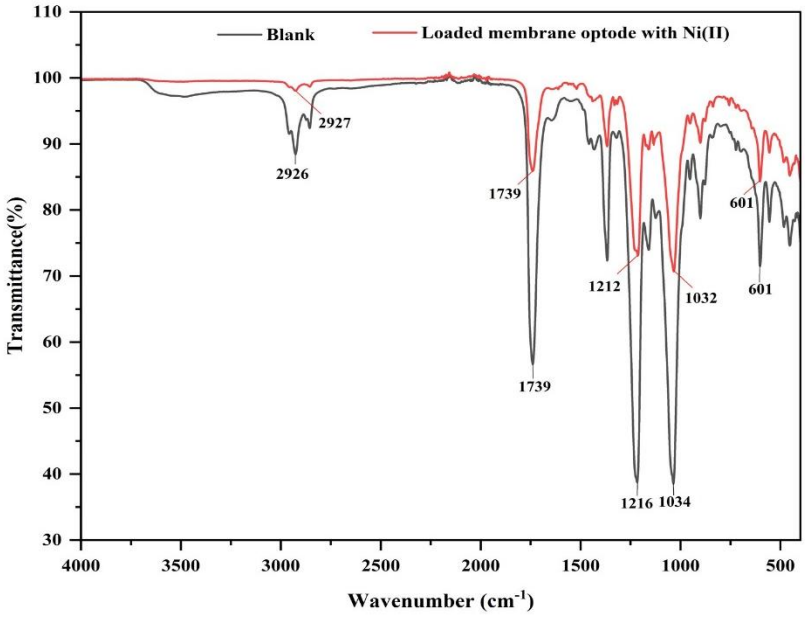


Fig. 4. FTIR spectra of (a) DecA, TBACl, DES (TBACl: DecA) 1:1 and (b) Blank and membrane loaded with Ni(II)

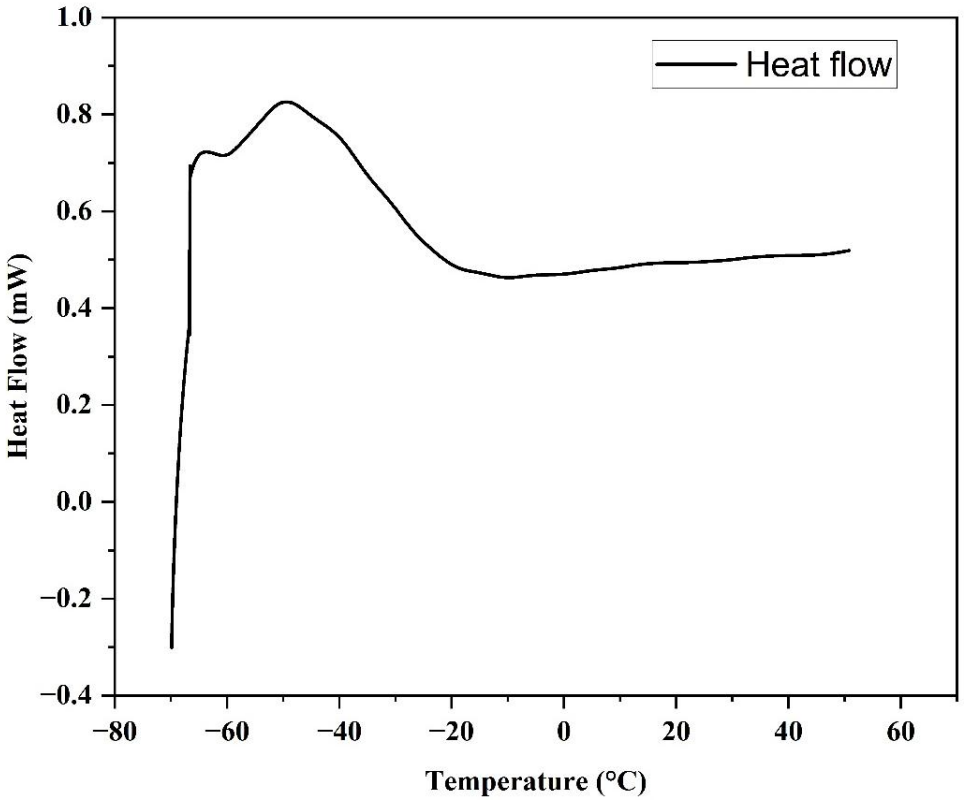
DSC analysis

Differential scanning calorimetry was performed to study the thermal behaviour of the DES-based membrane optode. The optode was heated from −70 °C to 50 °C at 10 °C/min. The DSC curve (Fig. 5(a)) shows a glass transition at approximately −66 °C, followed by a broad endothermic event that begins at about −55 °C, peaks near −25 °C and returns to the baseline near −10 °C; this event can be attributed to the melting of the DES dispersed in the polymer matrix. No sharp crystallization or melting peaks of crystalline components were observed, indicating that the membrane remains largely amorphous over the temperature range studied. Such glass-forming behaviour makes the membrane resistant to crystallization of the DES[53].

TGA Analysis

To determine the thermal stability of the DES-loaded membrane optode, thermogravimetric analysis was performed from room temperature to 600 °C under nitrogen at a heating rate of 10 °C/min (Fig. 5(b)). The membrane showed three main stages of weight loss, with most of the degradation occurring between 260 °C and 380 °C. The first stage, a minor weight loss of 10.22% between 102 °C and 190 °C, corresponds to the loss of absorbed moisture and residual dichloromethane from membrane casting[54,55]. The second stage, a weight loss of 16.57% between 190 °C and 260 °C, is attributed to the decomposition of the DES, and the third, major weight loss of 61.63% between 260 °C and 380 °C corresponds to the decomposition of the cellulose triacetate backbone. Above 380 °C and up to 600 °C, the remaining material undergoes slow carbonization, leaving a char residue[56]. Hence, apart from the loss of moisture and residual solvent, the membrane optode is thermally stable up to about 190 °C, well above the temperatures encountered in its intended application.

(a)



(b)

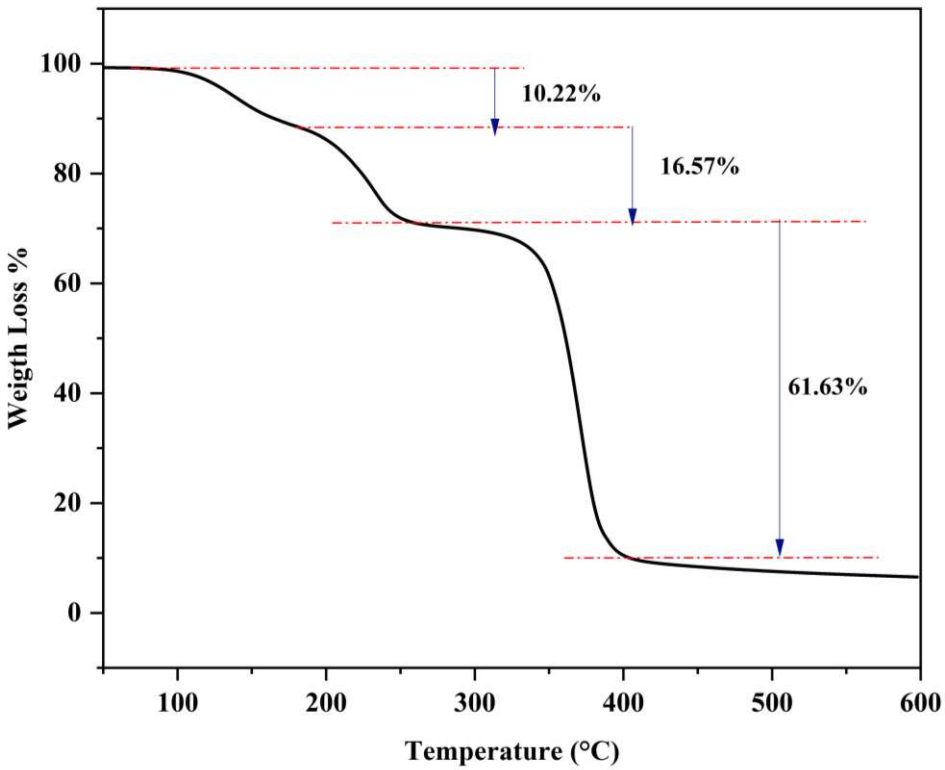


Fig. 5. (a) DSC thermogram of blank membrane optode, (b) TGA thermogram of blank membrane optode

FESEM studies

The cross-section and morphology of the prepared membrane optode were examined by field emission scanning electron microscopy (FESEM), with images recorded at scale bars of 2 µm and 10 µm. Fig. S4(a) corresponds to the cross-sectional FESEM images and EDX spectra of the DES-loaded blank membrane optode and Fig. S4(b) corresponds to the cross-sectional FESEM images and EDX spectra of the membrane optode loaded with 2.5 µg/mL of Ni(II) at pH 6. The membrane thickness was 34.67 µm, which provided adequate mechanical stability and a uniform surface. The blank membrane appears smooth and featureless. EDX for blank membrane optode in Fig. S4(a) and elemental mapping of the blank membrane optode in Fig. S4(c) show the presence of C, O and Cl; Cl originates from TBACl. The EDX and elemental mapping of Ni(II) loaded membrane optode shown in Fig. S4(b) and Fig. S4(d), respectively, when compared to the blank membrane optode, indicate the interaction between Ni(II) and the membrane optode components and confirm the adsorption of Ni(II) on the surface.

Atomic Force Microscopy

To further understand the surface morphology, atomic force microscopy (AFM) was performed for the membrane optode. 3D images of the surface (5 µm × 5 µm scan area) of the membrane without DES, with DES and after exposure to Ni(II) are shown in Fig. 6. The surface features correspond to elongated pores, or cavity channels, which can be attributed to the crystallinity of CTA[57]. The membrane optode, composed only of CTA and PAN without DES, exhibits some notable peaks and roughness features that may be due to the heterogeneous distribution of PAN molecules in the membrane, as well as to the aggregation of the CTA and PAN complex in the polymer matrix[58]. After incorporation of DES in the polymer membrane, the roughness decreased and a smoother surface was observed. The DES acts as a plasticizer, which facilitates the even distribution of PAN, resulting in fewer peaks and a smoother surface of the membrane[59]. After equilibration in the Ni(II) solution, the roughness increased, which can be attributed to Ni–PAN complexation causing restructuring within and at the surface of the membrane. Zang et al. also reported an increase in membrane surface roughness after exposure to metal ions[60]. The roughness values of the three membranes are compiled in Table S5.

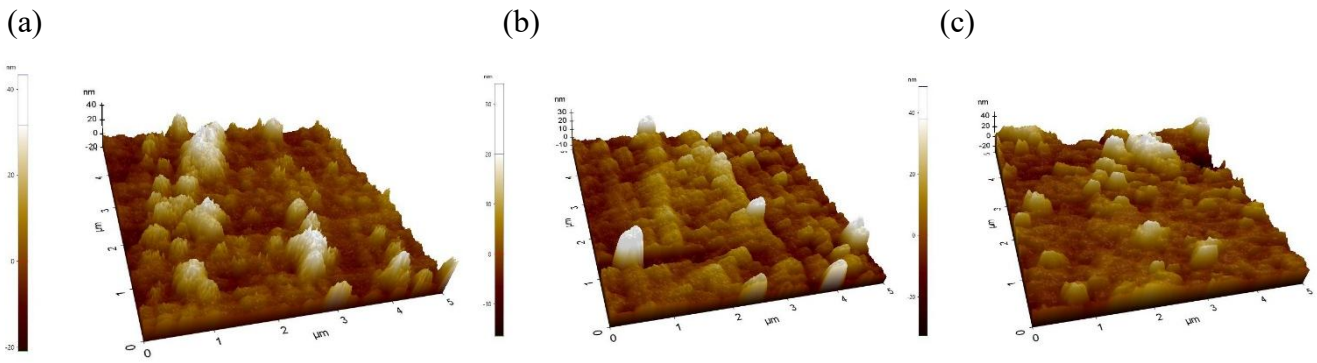


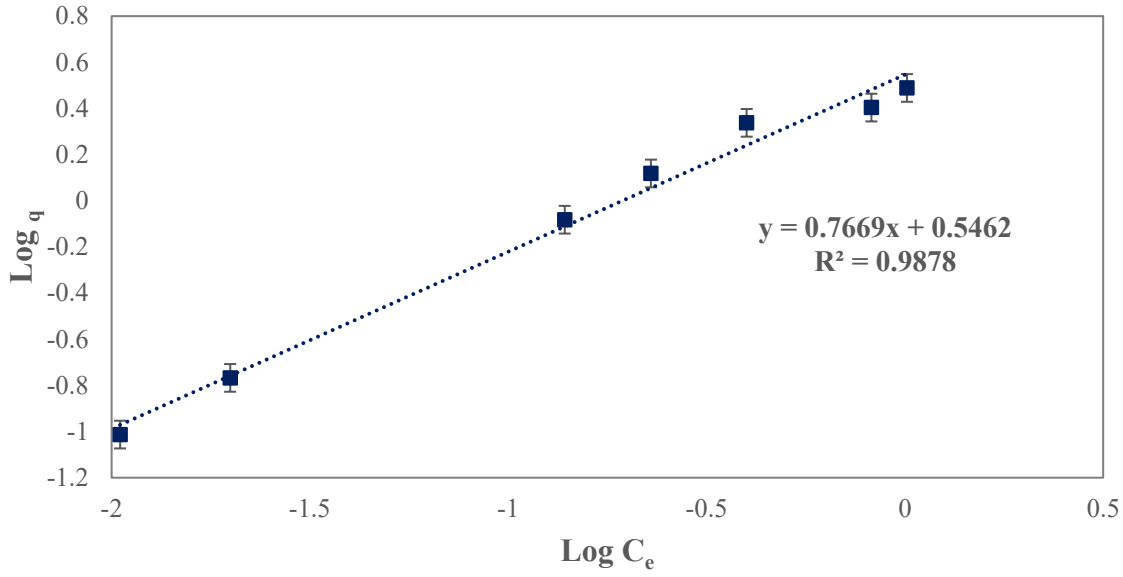
Fig. 6. AFM images of (a) membrane optode without DES, (b) blank membrane optode with DES and (c) DES membrane optode loaded with 2.5 µg/mL Ni(II) solution.

Adsorption isotherm studies

The adsorption isotherm was obtained using membrane optodes (2 cm × 1 cm; average weight 0.012 g) equilibrated with Ni(II) solutions from 0.05 µg/mL to 2.5 µg/mL at pH 6, and is shown in Fig. S5.

In order to understand the adsorption process, the data were fitted to the Freundlich and Langmuir isotherm models (Fig. 7(a) and 7(b), respectively), and the isotherm parameters are summarized in Table 1. As seen from Table 1, the adsorption of Ni(II) at pH 6 is better described by the Freundlich model ($R^2 = 0.988$) than by the Langmuir model ($R^2 = 0.962$). The value of 1/n (0.767) lies between 0 and 1, indicating favourable adsorption. Here, in addition to describing the energy distribution and heterogeneity of adsorption sites, 1/n is a measure of adsorption intensity[61].The maximum adsorption capacity of the membrane optode obtained through Langmuir isotherm is 4.45 mg/g. The R_L values (0.17–0.91) obtained from the Langmuir model also lie within the favourable range of 0 to 1. Based on the R^2 values, the Freundlich isotherm describes the data better than the Langmuir isotherm, suggesting multilayer adsorption of Ni(II) on a heterogeneous surface of the membrane optode.

(a)



(b)

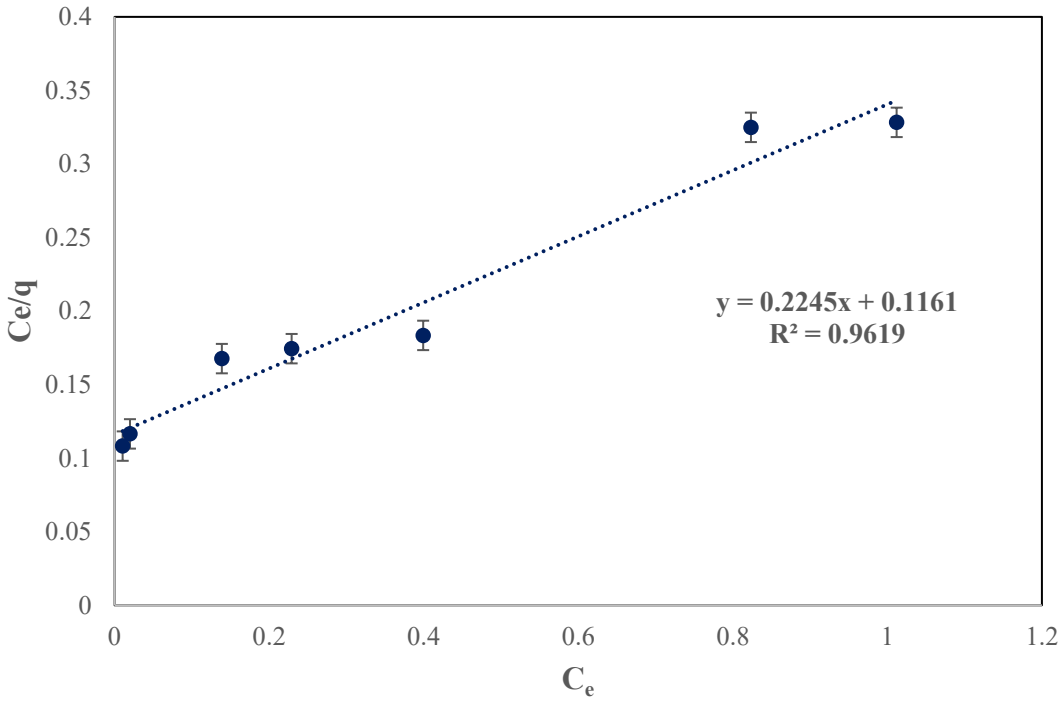


Fig. 7. (a) Freundlich isotherm and (b) Langmuir isotherm models for the Ni(II) adsorption onto the membrane optode.

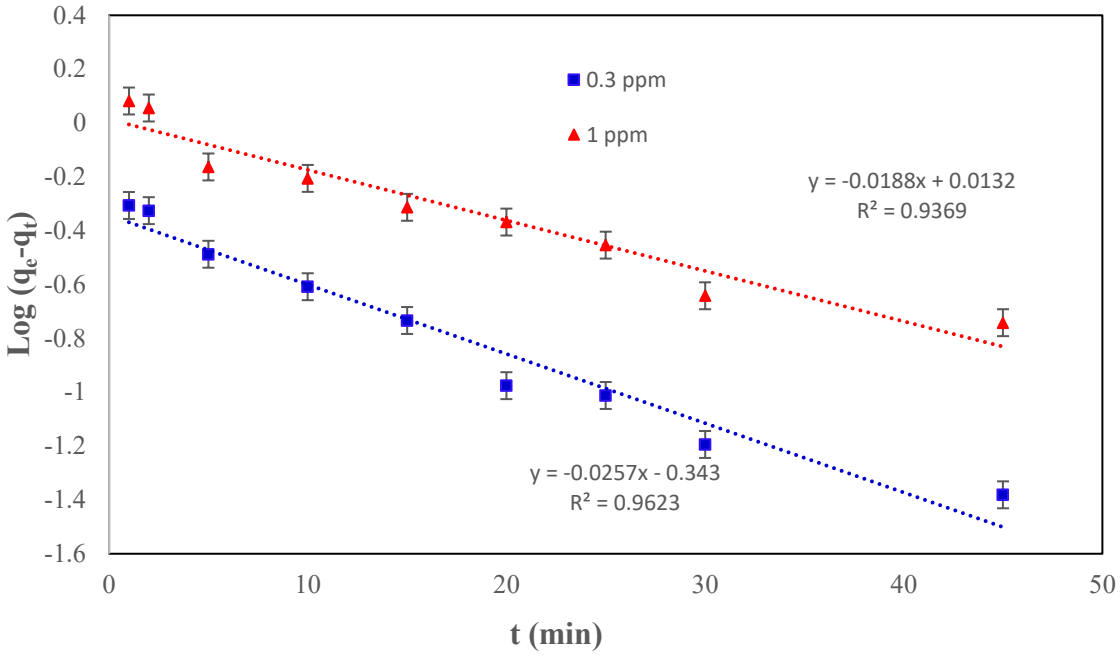
Table 1. Freundlich and Langmuir isotherm parameters for the adsorption of Ni(II) on the membrane optode.

Freundlich isotherm			Langmuir isotherm			
1/n	K (mg/g) $(L/mg)^{1/n}$	R^2	a (L/mg)	b (mg/g)	R_L	R^2
0.7669	3.52	0.988	1.934	4.454	0.17–0.91	0.962

Adsorption kinetics

To understand the rate of Ni(II) adsorption onto the membrane optode, the experimental data were fitted to the pseudo-first-order (Eq. 4) and pseudo-second-order (Eq. 5) kinetic models. The uptake of Ni(II) as a function of time at 0.3 µg/mL and 1 µg/mL is shown in Fig. S6. The pseudo-first-order and pseudo-second-order plots are given in Fig. 8(a) and 8(b), respectively, and the kinetic parameters are listed in Table 2. At 0.3 µg/mL, the pseudo-first-order model gave the higher R^2 (0.962 vs 0.799), and its calculated q_e (0.454 mg/g) was close to the experimental value (0.511 mg/g). At 1 µg/mL, the pseudo-second-order model fitted better (R^2 = 0.989 vs 0.937), with a calculated q_e (1.780 mg/g) close to the experimental value (1.729 mg/g). Thus, Ni(II) uptake at the lower concentration is adequately described by pseudo-first-order kinetics, whereas at the higher concentration pseudo-second-order kinetics applies, suggesting that chemical interaction (Ni–PAN complexation) becomes rate-controlling as the Ni(II) loading increases.

(a)



(b)

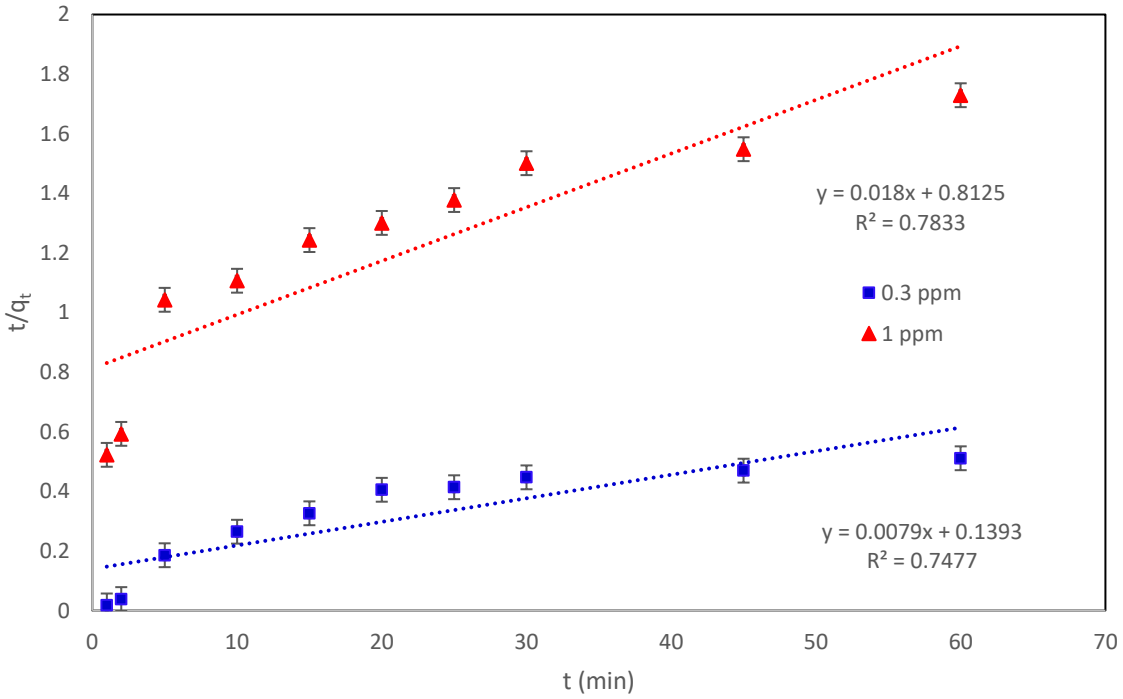


Fig. 8. (a) Pseudo-first order kinetics and (b) pseudo-second order kinetics for the adsorption of Ni(II) on the membrane optode

Table 2. Adsorption kinetics parameters for the adsorption of Ni(II) on the membrane optode.

Kinetic Models	Parameters	Concentrations (µg/mL)	
		0.3	1
Pseudo-first order	$q_{e,\,cal}$ (mg/g)	0.454	1.031
	$q_{e,\,exp}$ (mg/g)	0.511	1.729
	k_1 (min^{-1})	0.059	0.043
	R^2	0.962	0.937
Pseudo-second order	$q_{e,\,cal}$ (mg/g)	0.800	1.780
	$q_{e,\,exp}$ (mg/g)	0.511	1.729
	k_2 (g mg^{-1} min^{-1})	0.045	0.110
	R^2	0.799	0.989

Effect of interfering ions

In order to study the selectivity of the optode towards Ni(II), the effects of various cations and anions, namely Cd^{2+}, Na^{+}, K^{+}, Cr(VI), Mg^{2+}, Hg^{2+}, Pb^{2+}, Fe^{2+}, Cu^{2+}, F^{-}, Cl^{-}, NO_3^{-}, SO_4^{2-} were studied. The interference was studied by equilibrating the membrane optode in a solution containing a fixed amount of Ni(II) (2 µg/mL) with increasing mole ratios of interfering ions at pH 6. Thereafter, the absorbance of the membrane optode equilibrated in the solution containing interfering ions along with Ni(II) was compared to the absorbance of the membrane optode equilibrated in the solution of 2 µg/mL of Ni(II). The obtained results show that the ions Cd^{2+}, Na^{+}, K^{+}, Cr(VI), Mg^{2+}, F^{-}, Cl^{-}, NO_3^{-}, SO_4^{2-} did not interfere with the Ni(II) determination at up to 100-fold excess, and Hg^{2+} and Pb^{2+} were tolerated at up to 10-fold excess without any decrease in the response of the membrane optode. Within these tolerance limits, no significant deviation in the optical response was observed; the results are summarized in Table 3.

However, equimolar Fe^{2+} and Cu^{2+} interfered: Fe^{2+} decreased the response, whereas Cu^{2+} shifted λ_{max} from 568 nm to 557 nm, with a distinct colour change from yellow to violet. Fe^{2+} has chemical properties similar to those of Ni(II) and competes with it for complexation, hindering Ni(II) uptake[62]. The tolerance limit was taken as the concentration of interfering ion causing an error of not more than ±4.7% in the determination of Ni(II). These results show that the membrane optode can be used for the determination of Ni(II) in natural waters, provided that Fe^{2+} and Cu^{2+} are not present at comparable or higher concentrations. The EDXRF spectrum recorded in the presence of co-existing metals (Fig. S7) showed a dominant nickel

signal, with the characteristic Ni K_α and K_β observed at approximately 7.47 keV and 8.26 keV, respectively, indicating that nickel remained the major detectable element under the tested interference conditions and confirming the reliable identification of Ni(II) in the complex matrix.

Table 3. Effect of co-existing ions on the determination of Ni(II).

Interfering Ions	Tolerance Limit (Times)
Cd^{2+}, Na^{+}, K^{+}, Cr(VI), Mg^{2+}, F^{-}, Cl^{-}, NO_3^- SO_4^{2-}	100
Hg^{2+}, Pb^{2+}	10

Analysis of real water samples

Water samples (river water, industrial wastewater, electroplating wastewater and open-drain water) were collected in polyethylene bottles, acidified with HNO_3 to prevent precipitation of Ni(II), and stored at 4 °C. The samples were filtered through Whatman filter paper and then through a 0.2 µm syringe filter.

The applicability of the membrane optode was tested with these samples after adjusting them to pH 6. The samples were first analysed directly by ICP-MS, and the Ni(II) concentrations were found to be 0.45 µg/mL, 0.81 µg/mL, 0.57 µg/mL, 0.52 µg/mL, 0.53 µg/mL, 0.73 µg/mL in river water 1, river water 2, river water 3, industrial wastewater, electroplating wastewater and open-drain water, respectively. The background Ni(II) concentrations of the same samples determined with the optode by the standard addition method were 0.47 µg/mL, 0.85 µg/mL, 0.55 µg/mL, 0.57 µg/mL, 0.52 µg/mL and 0.74 µg/mL, respectively, in close agreement with the ICP-MS results (Table 4). Known concentrations of Ni(II) were then spiked into the samples (pH 6), and the concentrations were determined by the standard addition method[63]. The percentage deviation was calculated as |expected − found| / expected × 100, where the expected value is the sum of the background and added concentrations. The deviation ranged from 1.25% to 9.72%, indicating acceptable accuracy; the deviations may arise from other components of these complex matrices. These results validate the use of the membrane optode for real water samples.

Table 4

Determination of Ni(II) in real water samples using the developed membrane optode.

Samples	Background value (µg/mL) (Proposed method)	Found by ICP-MS (µg/mL)	Added (µg/mL)	Found (µg/mL) (Proposed method)	%Deviation
River water 1	0.47 ± 0.001	0.45 ± 0.01	0.25	0.65 ± 0.03	9.72
			0.75	1.16 ± 0.02	4.91
River water 2	0.85 ± 0.004	0.81 ± 0.02	0.25	1.2 ± 0.01	9.09
			0.75	1.58 ± 0.01	1.25
River water 3	0.55 ± 0.002	0.57 ± 0.02	0.25	0.78 ± 0.02	2.50
			0.75	1.21 ± 0.02	6.92
Industrial wastewater	0.57 ± 0.003	0.52 ± 0.008	0.25	0.86 ± 0.03	4.87
			0.75	1.30 ± 0.01	1.51
Electroplating wastewater	0.52 ± 0.001	0.53 ± 0.004	0.25	0.76 ± 0.05	1.29
			0.75	1.39 ± 0.04	9.44
Open drain	0.74 ± 0.002	0.73 ± 0.024	0.25	0.93 ± 0.02	6.06
			0.75	1.42 ± 0.02	4.69

Values are mean ± SD of three determinations.

Comparison with work reported in the literature

A comparison of the proposed membrane optode with previously reported methods for the determination of Ni(II) is given in Table 5. Although its detection limit is higher than those of some reported methods, the present optode does not require sophisticated instrumentation and gives a colour change visible to the naked eye within 30 min. It is also portable and easy to handle, and the use of a DES in the polymer matrix makes it a greener alternative. In addition, the membrane combines preconcentration and optical sensing of Ni(II) in a single step.

Table 5. Comparison of the present membrane optode with those reported in the literature.

Membrane type	Active component	Linear range and LOD	Application	Reference
Permeation liquid membrane	2-HBET in toluene	LR: 3-500 µg L^{-1} LOD: 0.012 µg L^{-1}	Natural and sea water	[64]
Plasticized PVC membrane	2,5-thiophenylbis(5-tert-butyl-1,3-benzoxazole) (TTBB)	LR: 1×10^{-8} - 1×10^{-3} mol L^{-1} LOD: 8×10^{-9}mol L^{-1}	Edible oil and wastewater samples	[65]
PVC matrix	Fluorescent thiazolo-triazole derivative	LR: 1×10^{-9}- 4.4×10^{-3} mol L^{-1} LOD: 8.5×10^{-10} mol L^{-1}	Tea leaves and wild edible mushrooms	[66]
Agarose membrane	Thionine	LR: 1×10^{-10} - 1×10^{-7} mol L^{-1} LOD: 9.30×10^{-11} mol L^{-1}	Natural water	[67]
PVC membrane	5-(2-benzothiazolylazo)-8-hydroxy-quinoline (BTAHQ)	LR: 2.5 - 110 ng mL^{-1} LOD: 0.75 ng mL^{-1}	Food and water samples	[68]
PVC	1-(2-pyridylazo)-2-naphthol and sodium tetraphenylborate	LR: 1.7 – 85.2 µmol L^{-1} LOD: 0.17 µmolL^{-1}	River water, mineral water, and hydrogen peroxide solutions	[69]
Silver nanoparticles	11MUA-modified AgNPs	LR: 3-7 µM LOD: 2.15 µM	Water	[70]
CTA membrane	PAN with (DES) Tetrabutylammonium chloride: Decanoic acid (1:1)	LR: 0.05 µg/mL – 2.5 µg/mL LOD: 0.03 µg/mL	River, industrial, electroplating and open-drain water	Present work

LR: linear range; LOD: limit of detection

Conclusion

A colorimetric membrane optode was developed by immobilizing 1-(2-pyridylazo)-2-naphthol (PAN) together with a tetrabutylammonium chloride–decanoic acid (1:1) deep eutectic solvent (DES) within a cellulose triacetate (CTA) matrix for the determination of Ni(II). The DES functioned simultaneously as extractant and plasticizer, facilitating Ni(II) uptake while imparting good mechanical flexibility to the membrane and removing the need for separate additives. The optode responded selectively to Ni(II) with a visible yellow-to-magenta colour change, giving a linear range of 0.05–2.5 μg/mL, a limit of detection of 0.03 μg/mL, and an equilibration time of 30 min at pH 6. FTIR confirmed hydrogen-bonding interactions between the DES components and their subsequent interaction with adsorbed Ni(II). TGA and DSC established the thermal stability of the membrane, and FESEM-EDX together with elemental mapping confirmed Ni(II) uptake by the membrane. AFM showed that incorporating DES reduced the surface roughness of the CTA-PAN membrane, while subsequent Ni(II) adsorption increased it again, consistent with restructuring driven by Ni-PAN complexation. Adsorption of Ni(II) fitted the Freundlich isotherm (R^2 = 0.988) better than the Langmuir model (R^2 = 0.962), indicating multilayer adsorption on a heterogeneous surface, and followed pseudo-first-order kinetics at 0.3 μg/mL and pseudo-second-order kinetics at 1 μg/mL. The optode retained its selectivity for Ni(II) in the presence of a wide range of co-existing cations and anions, tolerating up to 100-fold excesses of most interfering ions, with only equimolar Fe^{2+} and Cu^{2+} causing interference. The optode was applied to river water, industrial wastewater, electroplating wastewater and open-drain water; background Ni(II) values agreed with ICP-MS results, and deviations for spiked samples were 1.25–9.72%. These results show that the DES–CTA membrane optode is a simple, low-cost platform for the simultaneous preconcentration and colorimetric detection of Ni(II) in water samples.

Data availability

Data will be made available on genuine request to the corresponding author.

References

1. Muñoz, A. & Costa, M. Elucidating the mechanisms of nickel compound uptake: A review of particulate and nano-nickel endocytosis and toxicity. *Toxicology and Applied Pharmacology.* **260**, 1–16. https://doi.org/10.1016/j.taap.2011.12.014 (2012).
2. Mitchell, E.J. & Frisbie, S.H. A comprehensive survey and analysis of international drinking water regulations for inorganic chemicals with comparisons to the world health organization's drinking water guidelines. *PLoS ONE*. **18(11)**, e0287937. https://doi.org/10.1371/journal.pone.0287937 (2023).
3. Genchi, G., Carocci, A., Lauria, G., Sinicropi, M. S. & Catalano, A. Nickel: human health and environmental toxicology. *IJERPH* **17**, 679. https://doi.org/10.3390/ijerph17030679 (2020).
4. Ghaedi, M., Ahmadi, F. & Shokrollahi, A. Simultaneous preconcentration and determination of copper, nickel, cobalt and lead ions content by flame atomic absorption spectrometry. *Journal of Hazardous Materials* **142**, 272–278. https://doi.org/10.1016/j.jhazmat.2006.08.012 (2007).
5. Carvalho, R. N. C. S. *et al.* Multi-element determination of copper, iron, nickel, manganese, lead and zinc in environmental water samples by ICP OES after solid phase extraction with a C18 cartridge loaded with 1-(2-pyridylazo)-2-naphthol. *Anal. Methods* **7**, 8714–8719. https://doi.org/10.1039/C5AY01929J (2015).
6. Jackson, S. L., Spence, J., Janssen, D. J., Ross, A. R. S. & Cullen, J. T. Determination of Mn, Fe, Ni, Cu, Zn, Cd and Pb in seawater using offline extraction and triple quadrupole ICP-MS/MS. *J. Anal. At. Spectrom.* **33**, 304–313. https://doi.org/10.1039/C7JA00237H (2018).
7. Yamini, Y., Amiri, N. & Karimi, M. Determination of trace elements in natural water using X-ray fluorescence spectrometry after preconcentration with powdered silica gel. *X-Ray Spectrometry* **38**, 474–478. https://doi.org/10.1002/xrs.1201 (2009).
8. Lum, T.-S., Tsoi, Y.-K. & Leung, K. S.-Y. Current developments in clinical sample preconcentration prior to elemental analysis by atomic spectrometry: a comprehensive literature review. *J. Anal. At. Spectrom.* **29**, 234–241. https://doi.org/10.1039/C3JA50316J (2014).
9. Jalbani, N. & Soylak, M. Separation–preconcentration of nickel and lead in food samples by a combination of solid–liquid–solid dispersive extraction using SiO2 nanoparticles, ionic liquid-based dispersive liquid–liquid micro-extraction. *Talanta* **131**, 361–365. https://doi.org/10.1016/j.talanta.2014.07.099 (2015).

10. Reclo, M., Yilmaz, E., Soylak, M., Andruch, V. & Bazel, Y. Ligandless switchable solvent based liquid phase microextraction of nickel from food and cigarette samples prior to its micro-sampling flame atomic absorption spectrometric determination. *Journal of Molecular Liquids* **237**, 236–241. https://doi.org/10.1016/j.molliq.2017.04.066 (2017).
11. Mandal, S. & Lahiri, S. A review on extraction, preconcentration and speciation of metal ions by sustainable cloud point extraction. *Microchemical Journal* **175**, 107150. https://doi.org/10.1016/j.microc.2021.107150 (2022).
12. Vergel, C., Montoya, R., Mendiguchía, C., García-Vargas, M. & Moreno, C. HF-LPME as a green alternative for the preconcentration of nickel in natural waters. *Anal Bioanal Chem* **404**, 665–670. https://doi.org/10.1007/s00216-012-5896-8 (2012).
13. Vázquez-Palomo, L., Montoro-Leal, P., García-Mesa, J. C., López Guerrero, M. M. & Vereda Alonso, E. Green chemistry: magnetic dispersive solid phase extraction for simultaneous enrichment and determination of V, Ni, Ti and Ga in water samples by HR-CS ETAAS. *Anal. Methods* **17**, 124–135. https://doi.org/10.1039/D4AY01809E (2025).
14. Rashid, M. & Singh, S. K. Ultra-trace level detection of nickel(II) ions in real water samples using surface anchored recognition probes at liquid crystal sensing platform. *Chemical Physics Letters* **829**, 140766. https://doi.org/10.1016/j.cplett.2023.140766 (2023).
15. Kalyan, Y. *et al.* Membrane optode for mercury(II) determination in aqueous samples. *Journal of Hazardous Materials* **166**, 377–382. https://doi.org/10.1016/j.jhazmat.2008.11.027 (2009).
16. Kalyan, Y., Pandey, A. K., Naidu, G. R. K. & Reddy, A. V. R. Membrane optode for uranium(VI) ions preconcentration and quantification based on a synergistic combination of 4-(2-thiazolylazo)-resorcinol with 8-hydroxyquinaldine. *Spectrochimica Acta Part A: Molecular and Biomolecular Spectroscopy* **74**, 1235–1241. https://doi.org/10.1016/j.saa.2009.09.045 (2009).
17. Almeida, M. I. G. S., Cattrall, R. W. & Kolev, S. D. Polymer inclusion membranes (PIMs) in chemical analysis - A review. *Analytica Chimica Acta* **987**, 1–14. https://doi.org/10.1016/j.aca.2017.07.032 (2017).
18. Hassan, N. & Amin, A. S. Membrane optode for uranium(VI) preconcentration and colorimetric determination in real samples. *RSC Adv.* **7**, 46566–46574. https://doi.org/10.1039/C7RA08942B (2017).
19. Yaacob, S. F. F. S., Olasupo, A. & Suah, F. B. M. Polymer inclusion membranes based Optode: Recent advances and perspectives. *TrAC Trends in Analytical Chemistry* **171**, 117498. https://doi.org/10.1016/j.trac.2023.117498 (2024).

20. Adigun, B., Thapaliya, B. P., Luo, H. & Dai, S. Ionic liquid-based extraction of metal ions *via* polymer inclusion membranes: a critical review. *RSC Sustainability* **2**, 2768–2780. https://doi.org/10.1039/D4SU00297K (2024).
21. Rabiei, M. R., Hosseini, M. & Xu, G. Deep eutectic solvents: A review on their sensing applications. *Microchemical Journal* **203**, 110909. https://doi.org/10.1016/j.microc.2024.110909 (2024).
22. Yang, C. *et al.* Research on extraction of valuable metals from solid waste by deep eutectic solvents - A review. *Process Safety and Environmental Protection* **197**, 107008. https://doi.org/10.1016/j.psep.2025.107008 (2025).
23. Lin, Z., Liu, X. & Jiao, B. Deep eutectic solvents-modified advanced functional materials for pollutant detection in food and the environment. *TrAC Trends in Analytical Chemistry* **159**, 116923. https://doi.org/10.1016/j.trac.2023.116923 (2023).
24. Sadeghi, A. & Pazuki, G. R. Separation of heavy metals using aqueous two-phase systems based on choline chloride/urea and betaine/urea deep eutectic solvents. *Sci Rep* **15**, 3948. https://doi.org/10.1038/s41598-025-86611-w (2025).
25. Fesliyan, S. & Altunay, N. Sugar based natural deep eutectic solvent liquid liquid microextraction for the determination of nickel and copper in food and water samples. *Sci Rep* **16**, 20233. https://doi.org/10.1038/s41598-026-51019-7 (2026).
26. Taghizadeh, M., Taghizadeh, A., Vatanpour, V., Ganjali, M. R. & Saeb, M. R. Deep eutectic solvents in membrane science and technology: Fundamental, preparation, application, and future perspective. *Separation and Purification Technology* **258**, 118015. https://doi.org/10.1016/j.seppur.2020.118015 (2021).
27. Sakamoto, T., Hanada, T., Sato, H., Kamisono, M. & Goto, M. Hydrophobic deep eutectic solvents for the direct leaching of nickel laterite ores: Selectivity and reusability investigations. *Separation and Purification Technology* **331**, 125619. https://doi.org/10.1016/j.seppur.2023.125619 (2024).
28. Rashid, S. N. *et al.* A kinetic study of ex-situ soil remediation by nickel extraction using natural deep eutectic solvent. *Environmental Technology* **45**, 4820–4833. https://doi.org/10.1080/09593330.2023.2283093 (2024).
29. Carreira, A. R. F. *et al.* Super concentrated HCl in a deep eutectic solvent as media for the integrated leaching and separation of metals from end-of-life lithium-ion batteries. *Chemical Engineering Journal* **475**, 146374. https://doi.org/10.1016/j.cej.2023.146374 (2023).
30. Tan, İ. Ş., Kılınç, Y., Zaman, B. T. & Bakırdere, S. Deep eutectic solvent-based simultaneous complexation and preconcentration of nickel in Antarctic lake water samples

for determination by flame atomic absorption spectrometry. *Environ Monit Assess* **195**, 309. https://doi.org/10.1007/s10661-023-10940-4 (2023).

31. Elahi, F. *et al.* Ultrasound-assisted deep eutectic solvent-based liquid–liquid microextraction for simultaneous determination of Ni (II) and Zn (II) in food samples. *Food Chemistry* **393**, 133384. https://doi.org/10.1016/j.foodchem.2022.133384 (2022).
32. Zinov'eva, I. V., Kozhevnikova, A. V., Milevskii, N. A., Zakhodyaeva, Yu. A. & Voshkin, A. A. Extraction of Cu(II), Ni(II), and Al(III) with the Deep Eutectic Solvent D2EHPA/Menthol. *Theor Found Chem Eng* **56**, 221–229. https://doi.org/10.1134/S0040579522020178 (2022).
33. Erbas, Z., Soylak, M., Yilmaz, E. & Dogan, M. Deep eutectic solvent based liquid phase microextraction of nickel at trace level as its diethyldithiocarbamate chelate from environmental samples. *Microchemical Journal* **145**, 745–750. https://doi.org/10.1016/j.microc.2018.11.039 (2019).
34. Sorouraddin, S. M., Farajzadeh, M. A. & Okhravi, T. Development of dispersive liquid-liquid microextraction based on deep eutectic solvent using as complexing agent and extraction solvent: application for extraction of heavy metals. *Separation Science and Technology* **55**, 2955–2966. https://doi.org/10.1080/01496395.2019.1666874 (2020).
35. Rad, A. S., Rahnama, R., Zakeri, M. & Jamali, M. R. Dispersive liquid–liquid microextraction based on green type solvents—"deep eutectic solvents"—for highly selective separation and efficient preconcentration of nickel in water samples. *J IRAN CHEM SOC* **16**, 1715–1722. https://doi.org/10.1007/s13738-019-01643-0 (2019).
36. Dayra, H. A., Abdelaal, M. Y., Khalifa, M. E. & Abdallah, A. B. Novel optical optode for selective detection and removal of ultra-trace level of mercury ions in different environmental real samples. *Sci Rep* **14**, 26400. https://doi.org/10.1038/s41598-024-76571-y (2024).
37. Scindia, Y. M., Pandey, A. K., Reddy, A. V. R. & Manohar, S. B. Chemically selective membrane optode for Cr(VI) determination in aqueous samples. *Analytica Chimica Acta* **515**, 311–321. https://doi.org/10.1016/j.aca.2004.03.074 (2004).
38. Meng, X. *et al.* Optical sensing membrane for determination of trace cadmium(II), zinc(II) and copper(II) based on immobilization of 1-(2-pyridylazo)-2-naphthol on polymer inclusion membrane. *Microchemical Journal* **162**, 105767. https://doi.org/10.1016/j.microc.2020.105767 (2021).

39. Alberti, G., Re, S., Tivelli, A. M. C. & Biesuz, R. Smart sensory materials for divalent cations: a dithizone immobilized membrane for optical analysis. *Analyst* **141**, 6140–6148. https://doi.org/10.1039/C6AN01560C (2016).
40. Shrivastava, K. C., Kumar, K. S. A., Sengupta, A., Ali, S. M. & Ramkumar, J. Reversible hydrophobic deep eutectic solvent-based uranyl-sensing optode film in aqueous streams: color transformation and reusability. *Anal. Chem.* **96**, 12658–12666. https://doi.org/10.1021/acs.analchem.4c01357 (2024).
41. Ge, D., Zhang, Y., Dai, Y. & Yang, S. Air-assisted dispersive liquid–liquid microextraction based on a new hydrophobic deep eutectic solvent for the preconcentration of benzophenone-type UV filters from aqueous samples. *Journal of Separation Science* **41**, 1635–1643. https://doi.org/10.1002/jssc.201701282 (2018).
42. Roh, H. *et al.* Removal studies of Cd(II) and explosive compounds using buffalo weed biochar-alginate beads. *Journal of Industrial and Engineering Chemistry* **26**, 226–233. https://doi.org/10.1016/j.jiec.2014.11.034 (2015).
43. Wang, T., Jiang, M., Yu, X., Niu, N. & Chen, L. Application of lignin adsorbent in wastewater Treatment: A review. *Separation and Purification Technology* **302**, 122116. https://doi.org/10.1016/j.seppur.2022.122116 (2022).
44. Tseng, R.-L., Wu, F.-C. & Juang, R.-S. Characteristics and applications of the Lagergren's first-order equation for adsorption kinetics. *Journal of the Taiwan Institute of Chemical Engineers* **41**, 661–669. https://doi.org/10.1016/j.jtice.2010.01.014 (2010).
45. Ho, Y.-S. Second-order kinetic model for the sorption of cadmium onto tree fern: A comparison of linear and non-linear methods. *Water Research* **40**, 119–125. https://doi.org/10.1016/j.watres.2005.10.040 (2006).
46. Alizadeh, K., Rezaei, B. & Khazaeli, E. An agarose based optical membrane sensor for selective monitoring of trace nickel ions. *Journal of Photochemistry and Photobiology A: Chemistry* **417**, 113371. https://doi.org/10.1016/j.jphotochem.2021.113371 (2021).
47. Coo, L. dlC., Cardwell, T. J., Cattrall, R. W. & Kolev, S. D. Study of the extraction of 1-(2′-pyridylazo)-2-naphthol from ethanol–water solutions into Nafion® membranes. *Analytica Chimica Acta* **392**, 201–211. https://doi.org/10.1016/S0003-2670(99)00221-4 (1999).
48. Wei, Q. Rapid and selective method for the spectrophotometric determination of nickel naphthenate in gasoline in a microemulsion. *Talanta* **45**, 957–961. https://doi.org/10.1016/S0039-9140(97)00196-3 (1998).

49. Cengiz, E. & Karahan, İ. H. Kβ-to-Kα X-ray intensity ratio studies on changes of valance electron structures of nickel in Ni–B/hBN composite coatings. *Radiation Physics and Chemistry* **192**, 109928. https://doi.org/10.1016/j.radphyschem.2021.109928 (2022).
50. Li, Z., Zhang, E., Li, W. & Liu, H. Tribological study of two ammonium chloride-decanoic acid deep eutectic solvents (DESs) as high-performance lubricants. *Friction* **12**, 2441–2457. https://doi.org/10.1007/s40544-024-0888-1 (2024).
51. Bernicot, B. *et al.* Design and characterization of novel hydrophobic eutectic solvents based on metal-extracting ligands. *Journal of Molecular Liquids* **427**, 127332. https://doi.org/10.1016/j.molliq.2025.127332 (2025).
52. Ali, H. H., Ghareeb, M. M., Al-Remawi, M. & Al-Akayleh, F. T. New insight into single phase formation of capric acid/menthol eutectic mixtures by Fourier-transform infrared spectroscopy and differential scanning calorimetry. *Trop. J. Pharm Res* **19**, 361–369. https://doi.org/10.4314/tjpr.v19i2.19 (2020).
53. Kamar, M. N., Paquin, L., Limanton, E., Lagrost, C. & Morineau, D. Thermal, dielectric, and electrochemical study of decanoic acid–tetrabutylammonium chloride deep eutectic solvent. *Comptes Rendus. Chimie* **27**, 5–14. https://doi.org/10.5802/crchim.368 (2026).
54. Drai, N., Abdellaoui, N., Saib, F., Arous, O. & Trari, M. Elaboration and characterization of new polymeric membrane based on cellulose triacetate, polyelectrolytes and dioctylephthalate as plasticizer. *Desalination and Water Treatment* **255**, 185–191. https://doi.org/10.5004/dwt.2022.28340 (2022).
55. Nurazzi, N. M. *et al.* Thermogravimetric analysis properties of cellulosic natural fiber polymer composites: a review on influence of chemical treatments. *Polymers* **13**, 2710. https://doi.org/10.3390/polym13162710 (2021).
56. El Alia, Bab Ezzouar, 16111, Algiers, Algeria *et al.* Preparation and characterization of polymer inclusion membranes based on biodegradable cellulose/algerian clay for heavy metals removal from wastewater. *Cellulose Chem. Technol.* **58**, 891–899. https://doi.org/10.35812/CelluloseChemTechnol.2024.58.78 (2024).
57. Radzyminska-Lenarcik, E. & Ulewicz, M. The application of polymer inclusion membranes based on cta with 1-alkylimidazole for the separation of zinc(ii) and manganese(ii) ions from aqueous solutions. *Polymers* **11**, 242. https://doi.org/10.3390/polym11020242 (2019).
58. Mohamad Idris, A. I., Mustapa Kamal, S. M., Sulaiman, A., Omar, R. & Mohammad, M. Passion fruit juice concentration using fabricated cellulose triacetate/celluloseacetate

forward osmosis membrane. *Food Res.* **8**, 10–16. https://doi.org/10.26656/fr.2017.8(4).540 (2024).

59. Elhamarnah, Y., Qiblawey, H. & Nasser, M. Synergistic effects of deep eutectic solvents on the morphology and performance of polysulfone ultrafiltration membranes. *Journal of Environmental Management* **370**, 122920. https://doi.org/10.1016/j.jenvman.2024.122920 (2024).
60. Zhang, X. *et al.* Advanced modified polyacrylonitrile membrane with enhanced adsorption property for heavy metal ions. *Sci Rep* **8**, 1260. https://doi.org/10.1038/s41598-018-19597-3 (2018).
61. Ayawei, N., Ebelegi, A. N. & Wankasi, D. Modelling and interpretation of adsorption isotherms. *Journal of Chemistry* **2017**, 1–11. https://doi.org/10.1155/2017/3039817 (2017).
62. Zarei, K., Atabati, M. & Malekshabani, Z. Simultaneous spectrophotometric determination of iron, nickel and cobalt in micellar media by using direct orthogonal signal correction-partial least squares method. *Analytica Chimica Acta* **556**, 247–254. https://doi.org/10.1016/j.aca.2005.06.051 (2006).
63. Hu, S. *et al.* Simultaneous determination of lead and cadmium in water by metal oxide framework complex-modified glassy carbon electrodes. *Microchemical Journal* **205**, 111154. https://doi.org/10.1016/j.microc.2024.111154 (2024).
64. Aouarram, A., Galindo-Riaño, M. D., García-Vargas, M., Stitou, M. & El Yousfi, F. A permeation liquid membrane system for determination of nickel in seawater. *Talanta* **71**, 165–170. https://doi.org/10.1016/j.talanta.2006.03.038 (2007).
65. Shamsipur, M. *et al.* Development of a new fluorimetric bulk optode membrane based on 2,5-thiophenylbis(5-tert-butyl-1,3-benzexazole) for nickel(II) ions. *Analytica Chimica Acta* **501**, 55–60. https://doi.org/10.1016/j.aca.2003.09.008 (2004).
66. Aksuner, N., Henden, E., Yilmaz, I. & Cukurovali, A. A novel optical chemical sensor for the determination of nickel(II) based on fluorescence quenching of newly synthesized thiazolo-triazol derivative and application to real samples. *Sensors and Actuators B: Chemical* **166–167**, 269–274. https://doi.org/10.1016/j.snb.2012.02.059 (2012).
67. Hashemi, P., Hosseini, M., Zargoosh, K. & Alizadeh, K. High sensitive optode for selective determination of Ni2+ based on the covalently immobilized thionine in agarose membrane. *Sensors and Actuators B: Chemical* **153**, 24–28. https://doi.org/10.1016/j.snb.2010.09.068 (2011).

68. Alluhayb, A. H., Younis, A. M., Babalghith, A. O. & Amin, A. S. Eco-friendly optical sensor membrane for nickel ion detection in water and food samples. *Results in Chemistry* **13**, 102007. https://doi.org/10.1016/j.rechem.2024.102007 (2025).
69. Babaee, S., Pakdehi, S. G. & Nabavi, A. S. An optical chemical sensor for monitoring of nickel in waters and hydrogen peroxide samples. *JNDC* **1**, 58–69. https://doi.org/10.14302/issn.2377-2549.jndc-16-1212 (2016).
70. Rossi, A. *et al.* Silver Nanoparticle-based sensor for the selective detection of nickel ions. *Nanomaterials* **11**, 1733. https://doi.org/10.3390/nano11071733 (2021).

Acknowledgements

N.Y. is grateful to the National Fellowship for Other Backward Classes (NFOBC) for financial assistance (reference letter no. NBCFDC/E-70291). All the authors thank, University Science Instrumentation Centre (USIC), University of Delhi and Common Experiment Facility, Department of Physics, University of Delhi for providing the necessary instruments.

Author contributions

N.Y. Writing-original draft, Investigation, Methodology, Visualization, Validation, Review and editing; K.Y. Writing-original draft, Conceptualization, Investigation, Methodology, Supervision, Validation, Review and editing; A.K.P. Validation**,** Writing-review and editing.

Declarations

Competing interests

The authors declare no competing interests.

Additional information

Supplementary Information is available

Correspondence and requests for materials should be addressed to K.Y

Supplementary Files

This is a list of supplementary files associated with this preprint. Click to download.

- SupplementaryInformationScientificReportsNYFinal06102026.docx